ELSEVIER

Journal of Hydrology 269 (2002) 65–78

Journal of Hydrology

www.elsevier.com/locate/jhydrol

An analytical–numerical approach to the hydraulics of floating debris in river channels

D. Bocchiola*, F. Catalano, G. Menduni, G. Passoni

DIIAR, Hydraulic Division, Politecnico di Milano 32, Piazza Leonardo da Vinci, I-20133 Milano, Italy

Abstract

A new simplified approach is developed for the channel flow dynamics under woody debris transport. A continuous carpet of debris is considered, covering a uniform stationary current. Due to the floating debris the shear stresses in the fluid domain are affected. As a result, the velocity profile is different from the free surface flow. The simple model proposed here is able to capture the essential features of flow response to woody debris transport. Velocity and stress profiles are analytically derived for laminar flow and compared with the zero debris condition. More realistic turbulent currents are simulated with the Reynolds equations where turbulent stresses are modeled by the simple mixing length concept. Validation is carried out by comparison with experimental velocity profiles and with direct numerical simulation of the Navier Stokes Equations. Synthetic diagrams are proposed for the calculation of the flow velocity and the bed shear stresses in terms of the relevant non-dimensional parameters.

Keywords: Floating debris; Shear stress; Reynolds equation

1. Introduction

The study of floating debris, or drift, is a far reaching matter, with several implications in river basin evolution and management. Floating debris transport is mainly woody debris (Keller and Swanson, 1979; Andrus et al., 1988), showing to be one of the major issues in the dynamics of the fluvial environment (Abbe and Montgomery, 1996). Any obstruction in a river, say a bend or a narrow section, can trigger the progressive growth of floating vegetation hips, giving rise in a relatively short time to debris dike, producing considerable backwater effect and altering the local channel hydraulics (Young, 1991). During relevant flood events, the flooding risk, i.e. the risk that the water depth exceeds a given level, could be significantly increased by the presence of stagnating debris. The sudden breakdown of these dikes can induce peak discharges down-stream, higher than those expected in ordinary conditions. With their linear momentum logs and trunks represent a risk in case of collision with a solid structure, say dam walls or bridge piles (Diehl, 1997), also leading to relevant economic damages. Both natural and anthropic transport of wooden trunks, moving large amounts of bulk debris, interact with the fluvial environment on a short term, by altering the dynamics of flow as well as on a long term, by changing the erosion and sedimentation pattern of the river. Several studies have been directed to assess the yielding capacity of river basins in term of woody debris (for a discussion on the origin of woody debris, see e.g.

* Corresponding author. Tel.: +39-2-2399-6233; fax: +39-2-2399-6207.

E-mail address: daniele.bocchiola@polimi.it (D. Bocchiola).

0022-1694/02/$ - see front matter © 2002 Published by Elsevier Science B.V.
PII: S0022-1694(02)00195-6

Nomenclature

A^* Van Driest's near wall dampening constant, no unit
d water depth in presence of debris (m)
$d^* = d/h_0$ dimensionless water depth, related to h_0, no unit
h_0 uniform flow depth, no debris (m)
h_d debris thickness (m)
$h_d^* = h_d/d$ dimensionless debris thickness, related to d, no unit
$h^* = \rho_d h_d/(\rho h_0)$ dimensionless debris thickness, related to h_0, no unit
i channel slope (mm^{-1})
K Von Karman's constant
Q discharge per unit width ($m^2\ s^{-1}$)
$Q^* = Q/\nu$ dimensionless discharge per unit width, no unit
$R^* = u_f d/\nu$ Reynolds number of friction in presence of debris, no unit
$T^* = \tau_f/\tau_0$ shear stress ratio in presence of debris, no unit
u time averaged local velocity ($m\ s^{-1}$)
$u_f = \sqrt{\tau_f/\rho}$ friction velocity at channel bottom ($m\ s^{-1}$)
$u^* = u/u_f$ dimensionless time averaged local velocity, no unit
W channel width (m)
y wall distance (m)
$y^* = yu_f/\nu$ dimensionless wall distance, no unit
γ fluid specific weight ($N\ m^{-3}$)
γ_d debris specific weight ($N\ m^{-3}$)
ρ fluid density ($kg\ m^{-3}$)
ρ_d debris density ($kg\ m^{-3}$)
$\rho_d^* = \rho_d/\rho$ dimensionless debris density, no unit
$\tau_0 = h_0\gamma i$ shear stress at the channel bottom, no debris (Pa)
$\tau_i = h_d\gamma_d i$ shear stress at the debris–water interface (Pa)
$\tau_f = d\gamma i + h_d\gamma_d i$ shear stress at the channel bottom, debris (Pa)
$\chi = \tau_i/\tau_f$ shear stress ratio, no unit
ν fluid cinematic viscosity ($m^2\ s^{-1}$)

Lienkaemper and Swanson (1987)). Relations are also available for estimating the size of the trunks conveyable by the river, depending on its geometry (Harmon et al., 1986; Bilby and Ward, 1989). Several devices have also been tested in order to capture moving debris (Perham, 1987, 1988; Ginanni et al., 2000). The design of these devices requires deep knowledge about the debris dynamics. The bed erosion, which depends on the shear and velocity field (Shields, 1936; Egiazaroff, 1965; Yalin, 1982), is also altered by the effect of woody debris transport, stagnation and eventually removal (Murgatroyd and Ternan, 1983; Shields and Gippel, 1995). Not at last, woody jams are strictly connected with the development of fluvial wildlife (see e.g. Bryant (1983) about the influence of woody debris on fishery). The issue of woody debris formation and conveyance is therefore of utmost interest, for several reasons and by several points of view. With reference to river hydraulics, some literature is devoted to understand the transportation patterns of logs or trunks (Braudrick et al., 1997; Braudrick and Grant, 2000; Manga and Kirchner, 2000) and changes in hydraulic properties, due to local disturbance of the current, such as trunks, or logs jams (Young, 1991; Shields and Gippel, 1995; Abbe and Montgomery, 1996; Ginanni et al., 2000). The paper presented here is devoted to a general, simple framework of analysis of hydraulic conditions in presence of the external

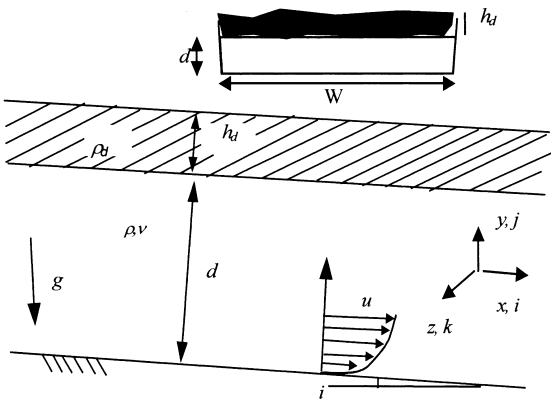

Fig. 1. Simplified scheme of floating debris carpet.

forcing due to floating debris. The issue of a uniform, stationary flow, covered by floating material is analyzed. The simplifying hypothesis of a continuous, inflexible carpet of debris is introduced. Under such assumption, the water flow is subjected to an additional drag force, due to the debris carpet. The bottom shear stress associated with a given discharge changes from the value under uniform flow conditions, thus affecting the bed load. The channel conveyance also changes, affecting the velocity field and water depth. The problem is first approached by considering low Reynolds number flows, which allows a closed form solution. Even though different from real channel flows, this approach enlightens the mechanics of the water flow. When turbulent flow is considered, no strictly analytic approach is possible. The momentum equation is rewritten in its time-averaged form, or Reynolds equation. The turbulent terms are modeled by a simple approach, allowing a straightforward numerical solution of the flow field. The model is validated through experimental measurements for Couette (air) flow (El Telbany and Reynolds, 1980) and an experiment according to direct numerical simulation (DNS). The turbulence model is used to assess differences in the rating curves and the shear stress patterns due to the presence of floating debris. Synthetic diagrams are shown and simple formulas proposed, which summarize the main results and also give a first picture of the complex dynamics in channels with floating debris.

2. Proposed approach

2.1. Simplified scheme

The problem is sketched in Fig. 1, where a continuous carpet of debris is floating over a uniform, stationary flow. The geometry of the channel is shown in Fig. 1; a very wide channel is considered and a quasi two-dimensional (2D) flow is assumed. This approximation is valid when the channel has a width much larger than its depth ($W > 5–6d$), and the motion is approximately 2D (Knight and Patel, 1985; Rhodes and Knight, 1994). This frequently happens during intense flood events, when the stream carries a large amount of debris, or when logs and trunks are conveyed for human activities. The carpet structure is continuous, i.e. no 'porosity' is considered and water entrapment into the debris structure is neglected, as well. It is also assumed that no other forces act over the debris, apart from its weight and the stresses at the interface with the underlying water. Other external forcing like wind stresses and side shears are not considered in this case, according to the local scale of the analysis and the 2D approach. The linear momentum equation in the flow direction gives the tangential stress acting on the interface between the wood carpet and the water layer

$$\tau_i = h_d \gamma_d i \quad (1)$$

where h_d is the debris carpet height, γ_d the debris specific weight and i the channel slope.

Generally speaking, the composition of woody debris carried by creeks and rivers is variable. The specific weight of the logs depends on wood type, age and moisture content (Braudrick et al., 1997), and is generally observed to range from about 3 to 6 kN m^{-1}. The debris height or diameter is even more variable and depends on the type of debris. Indeed, it can range from short logs, with a diameter of few centimeters, to the size of whole trees, dropped or eradicated by wind during storms, with several meters length and up to 1 or 2 m in diameter, also considering the size of canopy and roots (Braudrick et al., 1997; Diehl, 1997). Also, the motion patterns of woods are different (Braudrick and Grant, 2000). Trees with huge roots can actually 'dredge' the bottom and therefore move very slowly and bend their tracks (Abbe and Montgomery, 1996), while light,

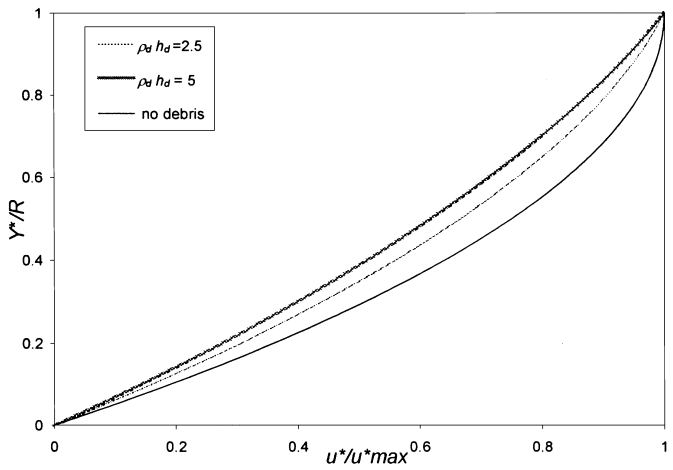

Fig. 2. Modified velocity profiles for laminar flow.

buoyant logs can follow the main current, also depending on the presence of river bends and meanders (for an experimental study, see, e.g. Ginanni et al. (2000)). The simplifying hypothesis that the current is straight is made; hence the motion is uniform in space and the debris follows the channel track. The shear stress in Eq. (1) is the upper boundary condition for the flow problem. This is different from the free-surface uniform flow. Applying the linear momentum equation on unit length fluid volume in the flow direction, the shear stress on channel's bed, τ_f is easily obtained

$$\tau_f = d\gamma i + h_d \gamma_d i = dg\rho i + h_d g \rho_d i, \tag{2}$$

where γ is the fluid specific weight and ρ its density. In order to cast the problem in non-dimensional form, some reference parameters have to be introduced. Considering the friction velocity at the channel bottom

$$u_f = \sqrt{\tau_f/\rho}, \tag{3}$$

it is possible to show (Yalin, 1971) that the averaged velocity profile, i.e. $u = u(y)$, into the channel can be properly described in terms of the following parameters

$$u^* = \frac{u}{u_f}; \qquad y^* = \frac{y u_f}{\nu}; \qquad R^* = \frac{u_f d}{\nu};$$
$$\rho_d^* = \frac{\rho_d}{\rho}; \qquad h_d^* = \frac{h_d}{d} \tag{4}$$

where Reynolds scaling has been applied.

2.2. Laminar flow

For a steady laminar flow, the projection of the momentum equation in the flow direction is:

$$\frac{\partial^2 u^*}{\partial y^{*2}} = -\frac{1}{R^*}\frac{1}{(1+\rho_d^* h_d^*)}. \tag{5}$$

After the first integration one obtains

$$\frac{\partial u^*}{\partial y^*} = -\frac{1}{R^*}\frac{1}{(1+\rho_d^* h_d^*)} y^* + C_1, \tag{6}$$

in which the boundary condition at the interface gives the constant C_1

$$y^* = \frac{u^* d}{\nu}; \qquad \frac{\partial u^*}{\partial y^*} = \frac{\tau_i}{\tau_f} = \frac{\rho_d^* h_d^*}{(1+\rho_d^* h_d^*)}; \tag{7}$$
$$C_1 = 1.$$

The equation for the velocity derivative then reads:

$$\frac{\partial u^*}{\partial y^*} = 1 - \frac{1}{R^*}\frac{1}{(1+\rho_d^* h_d^*)} y^*. \tag{8}$$

The tangential stress is a linear function of the y^* coordinate, as for free surface flows, but not vanishing at the upper layer. A further integration yields the non-dimensional velocity profile

$$u^* = y^* - \frac{1}{R^*}\frac{1}{(1+\rho_d^* h_d^*)}\frac{y^{*2}}{2} + C_2 \tag{9}$$

which has to be coupled with the no-slip condition

$$y^* = 0; \qquad u^* = 0; \qquad C_2 = 0. \tag{10}$$

The cross averaged velocity in the channel, U^* is

$$U^* = \frac{R^*}{2} - \frac{1}{(1+\rho_d^* h_d^*)}\frac{R^*}{6}. \tag{11}$$

For a given water depth, the vertically averaged velocity increases with the non-dimensional debris weight, i.e. $\rho_d^* h_d^*$. The dimensionless discharge is

$$Q^* = \frac{Q}{\nu} = U^* R^* = \frac{R^{*2}}{2} - \frac{1}{(1+\rho_d^* h_d^*)}\frac{R^{2*}}{6}, \tag{12}$$

where Q is the discharge per unit width. For a certain Q^* it is clear that a lower weight of debris requires a greater value of R^* hence a higher water depth. In Fig. 2 some velocity profiles are plotted, parameterized by $\rho_d^* h_d^*$. Increasing the debris weight the velocity profile becomes steeper, with a larger average velocity and a lower water depth. The debris velocity and its kinetic energy are related to the maximum value of u^*:

$$u_m^* = -\frac{1}{(1+\rho_d^* h_d^*)}\frac{R^*}{2} + R^*; \qquad E^* = \tfrac{1}{2} u_m^{*2} \rho_d^* h_d^*. \tag{13}$$

2.3. Turbulent flow

As in real river channels the flow is turbulent, the momentum equation must be rewritten. Denoting with $u^*(y^*)$ the time-averaged non-dimensional streamwise velocity, the Reynolds momentum conservation equation states

$$\frac{\partial^2 u^*}{\partial y^{*2}} - \frac{\partial(\overline{u'v'})^*}{\partial y^*} = -\frac{1}{(1+\rho_d^* h_d^*)}\frac{1}{R^*}, \tag{14}$$

where

$$\frac{\overline{u'v'}}{u_f^2} = \overline{u'v'}^{+}. \tag{15}$$

To solve Eq. (14) the second term on the LHS, i.e. the derivative of the turbulent stress, needs to be modeled. Several closures have been proposed for the Reynolds equations (see e.g. Wilcox (1993), for a review). In this context the authors were concerned in finding a simple model, able to capture the main features of the field, i.e. the velocity and stress profile. One of the firsts is the *mixing length* theory (Prandtl, 1925). The non-dimensional turbulent shear stress τ_t^* is expressed by

$$\tau_t^* = l^{*2}\left(\frac{\partial u^*}{\partial y^*}\right)^2 \tag{16}$$

where l^* is an appropriate length, modeling the turbulence at a given distance from the solid boundary. The parameter is usually assumed to depend upon the distance from the wall, through some relations (Schlichting, 1960; Shermann, 1990). According to Van Driest (1956), this can take into account the 'damping' effect on the turbulent stresses due to the proximity of the solid boundaries, and the mixing length exponentially decrease towards the wall:

$$l^* = K y^*\left(1 - \exp\left(-\frac{y^*}{A^*}\right)\right). \tag{17}$$

The parameter K is the well known Von Karman's constant ($K = 0.41$) and A^* is a parameter, to be calibrated with experimental data. For an undisturbed flow, $A^* = 26$ has been found (Van Driest, 1956; Chapman and Kuhn, 1986). The exponential expression on the RHS takes into account the damping effect near the wall and is usually valid inside the 'buffer' zone of the turbulent layer, where both viscosity and density are important in shear stress production. For this reason it has been used outside of the 'viscous sub layer' ($y^* > 5$) (Van Driest, 1956; Spalding, 1961). The velocity distribution in a turbulent layer is obtained after substituting the Van Driest approach in Eq. (14):

$$\frac{\partial^2 u^*}{\partial y^{*2}} + \frac{\partial\left[K^2 y^{*2}\left(1 - \exp\left(\frac{-y^*}{A^*}\right)\right)^2\left(\frac{\partial u^*}{\partial y^*}\right)^2\right]}{\partial y^*} = -\frac{1}{(1+\rho_d^* h_d^*)}\frac{1}{R^*}. \tag{18}$$

The velocity profile is easily obtained from Eq. (18), after imposing the proper stress condition on the upper boundary. For this purpose we state that, however the turbulent stress is modeled, it must vanish at the upper

boundary. Eq. (18) is integrated as follows:

$$\frac{\partial u^*}{\partial y^*} + K^2 y^{*2}\left(1 - \exp\left(\frac{-y^*}{A^*}\right)\right)^2\left(\frac{\partial u^*}{\partial y^*}\right)^2 = -\frac{1}{(1+\rho_d^* h_d^*)}\frac{1}{R^*}y^* + C_3. \quad (19)$$

To find the constant C_3 a further assumption has to be introduced. The development of turbulent stresses is affected by the limiting action of the wall. It is reasonable to assume that very close to the debris surface the motion is dominated by viscosity. For this reason we express the mixing length as a function of a variable y_n^* defined as

$$y_n^* = y^*(1 - y^*/R^*). \quad (20)$$

This variable allows the dampening to behave symmetrically inside the domain, and goes to zero at the solid boundaries. The momentum equation then becomes:

$$\frac{\partial u^*}{\partial y^*} + K^2 y_n^{*2}\left(1 - \exp\left(\frac{-y_n^*}{A^*}\right)\right)^2\left(\frac{\partial u^*}{\partial y^*}\right)^2 = -\frac{1}{(1+\rho_d^* h_d^*)}\frac{1}{R^*}y^* + C_3. \quad (21)$$

Eq. (21) is integrated and constant C_3 derived from the dynamical condition:

$$y_n^* = 0; \qquad \tau_t^* = K^2 y_n^{*2}\left(1 - \exp\left(\frac{-y_n^*}{A^*}\right)\right)^2\left(\frac{\partial u^*}{\partial y^*}\right)^2 = 0 \quad (22)$$

$$\frac{\partial u^*}{\partial y^*} = \frac{\tau_i}{\tau_f} = \frac{\rho_d^* h_d^*}{(1+\rho_d^* h_d^*)}; \qquad C_3 = C_1 = 1. \quad (23)$$

Leading to

$$K^2 y_n^{*2}\left(1 - \exp\left(\frac{-y_n^*}{A^*}\right)\right)^2\left(\frac{\partial u^*}{\partial y^*}\right)^2 + \frac{\partial u^*}{\partial y^*} = -\frac{1}{(1+\rho_d^* h_d^*)}\frac{1}{R^*}y^* + 1. \quad (24)$$

Eq. (18) is indeed the turbulent counterpart of Eq. (5) and only differs from it in the turbulent stress term. It states that the total (non-dimensional) shear stress, i.e. the sum of laminar (viscous) and turbulent stress, varies linearly from the maximum (one) value at the bottom to the minimum value at the interface with the debris. This is a quadratic equation in the derivative of the velocity

$$a\left(\frac{\partial u^*}{\partial y^*}\right)^2 + b\frac{\partial u^*}{\partial y^*} = c \quad (25)$$

where the coefficients a, b, c do not depend on the velocity derivative itself. The derivative is obtained by

$$\frac{\partial u^*}{\partial y^*} = \frac{-b \pm \sqrt{b^2 + 4ac}}{2a} \quad (26)$$

and the velocity profile admits the solution (Van Driest, 1956)

$$u^* = \int_0^{y^*} \frac{-1 + \sqrt{1 + 4K^2 y_n^{*2}\left(1 - \exp\left(\frac{-y_n^*}{A^*}\right)\right)^2\left(-\frac{1}{(1+\rho_d^* h_d^*)}\frac{1}{R^*}y^* + 1\right)}}{2K^2 y_n^{*2}\left(1 - \exp\left(\frac{-y_n^*}{A^*}\right)\right)^2} dy^* + C_4 \quad (27)$$

together with the boundary condition:

$$y^* = 0; \qquad u^* = 0; \qquad C_4 = 0. \quad (28)$$

Eq. (27) requires numerical integration and provides the non-dimensional velocity profile inside the domain. When no debris is present, the term containing $\rho_d^* h_d^*$ under the square root tends to one, being smaller otherwise. This means that, given u_f and the integral scale R^*, the velocity derivative tends to increase, compared with respect to the 'free' surface flow. The velocity profile for given values of u_f and R^* is steeper with debris than without it, i.e. the flow is faster in the former than in the latter case. The main difference with the laminar flow is the inflection in the

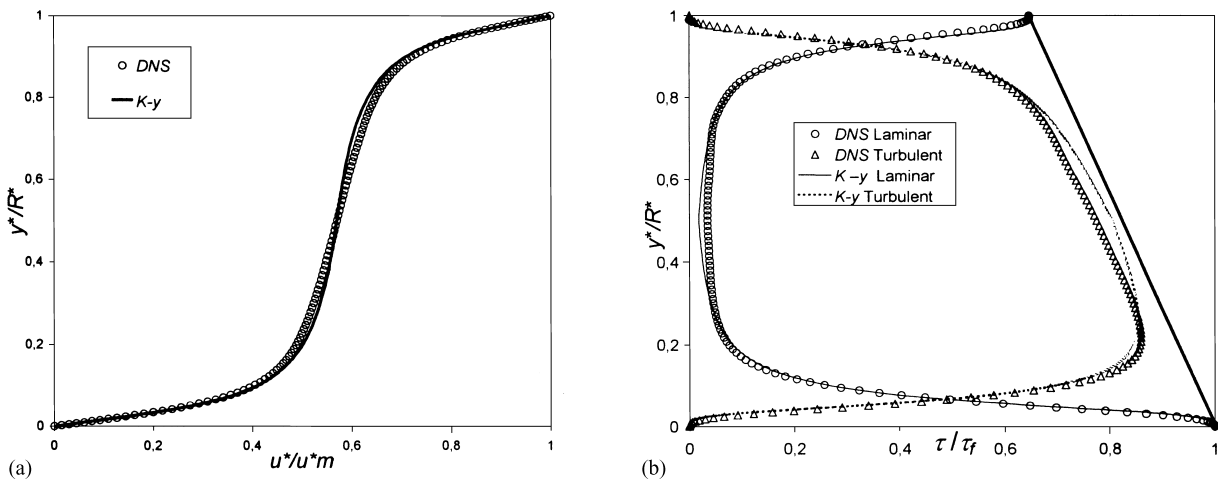

Fig. 3. (a) DNS, velocity profile; (b) DNS, shear stress profile.

velocity profile while the second velocity derivative for laminar flow (Eq. (5)) is always negative. The same derivative for turbulent flow in Eq. (18) has a zero value where:

$$\frac{\partial\left[K^2 y^{*2}\left(1-\exp\left(\frac{-y^*}{A^*}\right)\right)^2\left(\frac{\partial u^*}{\partial y^*}\right)^2\right]}{\partial y^*} = -\frac{1}{(1+\rho_d^* h_d^*)}\frac{1}{R^*}. \tag{29}$$

This equation requires the numerical calculation of the first derivative of velocity, thus not allowing a direct solution. Nevertheless, it is to expect that the velocity profile changes its concavity to a positive value at some point into the fluid domain, i.e. possess an inflexion point. This feature is indeed observed in velocity profiles related to flow conditions similar to the one here concerned, as will be shown in the following.

3. Model validation

3.1. Model validation with direct numerical simulation

A DNS has been carried out for the same fluid domain sketched in Fig. 1 This consists in numerically solving the full set of equations (i.e. Navier Stokes equations) describing the flow dynamics in its direct form. Due to the computational requirements, numerical simulation can only be carried out for low Reynolds numbers. While it is expected that most of the applications for the proposed research are related to fully turbulent flow conditions, where the Reynolds equations are expected to hold, it is nevertheless interesting to determine the main features of the flow field for an intermediate range of Reynolds numbers. The numerical simulation, which requires a notable effort and whose accurate description would possibly require a paper by itself, is here only shown in its main results (for a description of the numerical method, the reader is referred to Alfonsi et al. (1998) and Passoni et al. (1999)). The 3D computational domain was designed in order to capture most of the features of the turbulent flow, adopting the frame of reference in Fig. 1 The domain's dimension were set $L_x = 2\pi$, $L_y = 2$, $L_z = \pi$ in the stream-wise, vertical and a span-wise direction, respectively. The grid parameters were set to $N_x = 72$, $N_y = 129$, $N_z = 48$ modes/nodes adopting a hyperbolic tangent node stretching along the inhomogeneous (y) direction. Periodicity in the stream-wise and span-wise directions has been assumed via horizontal Fourier expansions. When compared, these figures are close, for similar Couette flows, to those reported by Lundbladh and Johansson (1991), apart from the additional gravity forcing considered in this specific case. The simulation has

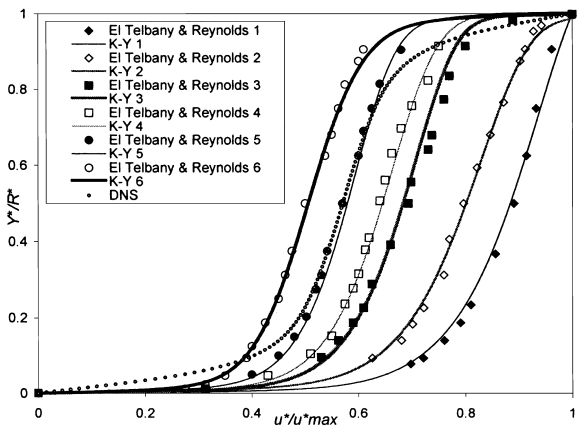

Fig. 4. Experimental profiles for non-symmetric Couette flow, in El Telbany and Reynolds (1980) and their fitting by turbulence model.

been started from a laminar stream-wise velocity profile on which random phase disturbances have been superimposed to reach a turbulent statistical steady state. The main flow characteristics (mean velocity and stress profile) have been computed after averaging over more than four integral time scale, after steady turbulent state was reached. After the statistically steady state was reached the friction Reynolds number R^* asymptotically resulted 310. The mean stream-wise velocity profile is shown in Fig. 3a while the companion Fig. 3b shows the shear stress inside the fluid domain. Together with the simulated field, the solution obtained by acting a tuning procedure of the turbulence model is reported here. In deeper detail, the A^* parameter in Eq. (17) is changed so that the (non-dimensional) velocity profiles obtained by the model has the minimum square error related to the DNS. The value of K in the turbulence model is not found to influence considerably the velocity distribution given by the model. The K parameter is therefore kept at its value 0.41. The value of A^* giving the best fitting is 136, which yields the maximum value of determination coefficient R, over the simulated values, 0.98. Also, a good determination coefficient, 0.99, is reached, related to non-dimensional stress into the field of motion. There is indeed a good fitting between the values obtained with the numerical simulation and with the $K-y$ model. As already stated, the required change in the turbulent model parameter is likely due to the friction number involved in the simulation, too low to fit well the $K-y$ model. Also, we will show in the following that the velocity profile developed in the simulation is not representative of a fully turbulent flow. The adopted value of A^* acts in a way to diminish the characteristic mixing length into the domain, so as to amount into a lower shear stress and a 'steeper' velocity profile, which is typical of viscous motion.

Table 1
Main properties of the experimental profiles. All variables are dimensionless

Exp.	χ	R^*	*Re* exp.	*Re* $K-y$
1	0.0057	2600	58×10^3	60×10^3
2	0.036	1400	38×10^3	30×10^3
3	0.116	1700	57×10^3	37×10^3
4	0.25	1600	57×10^3	36×10^3
5	0.5	1400	57×10^3	32×10^3
6	1	1300	57×10^3	29×10^3
DNS	0.65	300	8×10^3	8×10^3

3.2. Model validation with experimental velocity profiles

Due to the non-dimensional form of Eq. (27) it is expected that it can describe any velocity profile, properly scaled. In order to test such features, the authors compared some observed profiles, obtained by El Telbany and Reynolds (1980), for fully turbulent flow motion. Those profiles are actually related to a blown air flow into a duct, equipped with sliding walls, thus resulting into a non-symmetric stress field, similar to the one the paper deals with. Therefore, we show here how the proposed model adapts to the observed velocity profiles. In Fig. 4 the experimental velocity profiles are shown. For the sake of clearness, only six cases are shown, each other different in the ratio between the upper and lower shear stress, τ_i and τ_f:

$$\chi = \frac{\tau_i}{\tau_f} = \frac{h_d^* \rho_d^*}{h_d^* \rho_d^* + 1}. \tag{30}$$

It is seen from Eq. (27) that, once $\rho_d^* h_d^*$ and R^* are known, the dimensionless velocity profile is known as well. The experimental values of R^* have been therefore calculated. The obtained profiles are shown in Fig. 4 with solid lines. The main properties of the profiles are in Table 1 (see El Telbany and Reynolds

(1980) for a deeper insight). The integral Reynolds number is reported, $Re = dU/\nu$, related to the development of turbulence. A part from some scatter at the very edges of the flow field, where indeed a few measurements are available, it is seen that the proposed model fits well the velocity profiles. No numerical analysis was performed, due to the low number of measurements, but it is the opinion of the authors that the described model is sufficiently accurate to describe with good approximation the main features of the flow field.

It has to be noticed that the measured profiles actually show an inflexion point. Qualitatively, it can be stated that the greater the upper stress amount is, the closer is the flex to the middle point. When the shear stress is the same at both boundaries, the flex exactly matches the line of half field. When the inflexion point is reached, the first velocity derivative reaches a minimum, also spotted on the proposed graphs. Then, it starts growing, leading to a steeper velocity profile, i.e. increasing the amount of discharge conveyed by the fluid. The closer the flex is to the line of half field, i.e. the heavier the debris, the greater is the increase in velocity. In Fig. 4 the DNS velocity profile is also shown, having χ equal to 0.65. Such profile looks steeper than the other ones, i.e. the velocity derivative, directly linked to viscous shear stresses, is indeed greater than ones expects, by looking at the other profiles. As formerly introduced, this behavior is probably due to the low velocity, and Reynolds number, into the simulated channel. The someway higher values of the Reynolds number related to the experiments by El Telbany and Reynolds (1980) allows a more complete development of turbulence and they are therefore well described by the turbulence model. Although it is known that more complex turbulence models exist, able to explain not only first order statistics of motion, such as velocity and stress, but also higher order ones, it is their opinion that the use of the simple model yields results accurate enough at the hydrologic scale of the phenomena. On the basis of the observed results, the proposed model is reliable, for the evaluation of the velocity profile for turbulent flows in presence of floating debris. Furthermore, one has to notice that the Reynolds equations (14)–(29), are cast in a dimensionless form. The proposed turbulence model was also written in dimensionless form, hence suitable for more general applications. The model here proposed can be applied to any similar case, provided that the Reynolds number Re is high enough ($Re > \sim 10^4$) and its agreement with experimental data does fit better as Re increases. This possibly includes real channel flows, where Re up to 10^6–10^7 are expected.

Based on these findings, the model has been adapted to assess the influence of floating debris on the rating curves and the shear stress distribution for several conditions, some of which are similar to those in river channels.

4. Rating curves and bed shear

4.1. Laminar flow

In this section, we will show the influence of floating debris over the rating curves and the bed shear. We introduce the following non-dimensional variables

$$h^* = \frac{\rho_d h_d}{\rho h_0}; \qquad d^* = \frac{d}{h_0}; \qquad T^* = \frac{\tau_f}{\tau_0} \tag{31}$$

where h_0 is the free surface water depth for uniform flow and τ_0 is the bed shear. The h^* parameter is the ratio between the weight of the fluid in case of free surface flow and the superimposed debris weight. The d^* parameter in turn represents the ratio between the depth of the flow in presence of debris and the corresponding depth under free surface conditions. The T^* variable accounts for the variation of shear stress, when the debris is superimposed to the flow. The issue of determining the modified rating curves is reduced to the calculation of d^*, once Q^* and h^* are known. Roughly speaking, when the discharge in a channel and the related amount of debris are known, one wants to determine what the necessary water depth is to convey the fluid. By equating the dimensionless discharge in presence of debris to its counterpart for free surface conditions, modified rating curves i.e. d^* are obtained. For the case of laminar flow, an analytical form can be deduced to evaluate d^*. First, one calculates the discharge as a function of water depth for no debris and debris

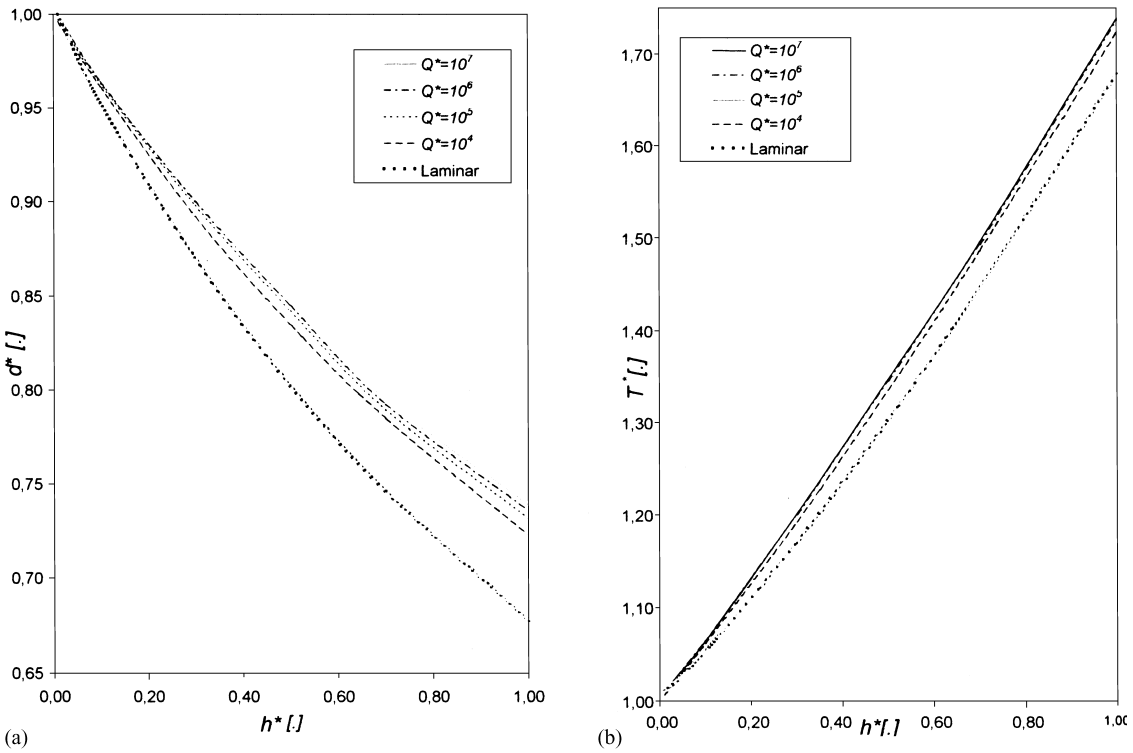

Fig. 5. (a) d^* vs. h^*; (b) T^* vs. h^*.

features. From Eqs. (11) and (31):

$$Q^* = -\frac{1}{(1+\rho_d^* h_d^*)}\frac{R^{*2}}{6} + \frac{R^{*2}}{2} = -\frac{d^*}{(d^*+h^*)}\frac{R^{*2}}{6} + \frac{R^{*2}}{2}. \quad (32)$$

Equating such discharge to its free surface counterpart, one obtains, after minor algebra:

$$\frac{d^{*3}}{3} + \frac{d^{*2}}{2}h^* - \frac{1}{3} = 0. \quad (33)$$

This equation can be solved to obtain the proper dimensionless flow depth. From a qualitative point of view, it is seen that the greater the debris weight, h^*, the smaller the depth d^*. Also, as h^* is non-negative by definition, d^* is always lower than, or at least equal to one, as it is expected. The stress ratio is given by

$$T^* = h^* + d^* = d^*\frac{1}{3} + \frac{2}{3}\frac{1}{d^{*2}}, \quad (34)$$

yielding T^* once Eq. (33) is solved. As d^* is always smaller than or at least equal to one, it is seen from Eq. (34) that T^* is always greater than or at least equal to one. Therefore, the bed shear stress is always increased by the presence of floating debris. This is shown here for the case of laminar flow, but the same results will be found for the turbulent flow later on in the paper. In a further section, a graphic representation of Eqs. (33) and (34) will be shown.

4.2. Turbulent flow

In case of turbulent flow, no analytical solution is available for the velocity profile and hence for d^*. Using dimensional arguments (Yalin, 1982), however, this reduces to the solution of the following

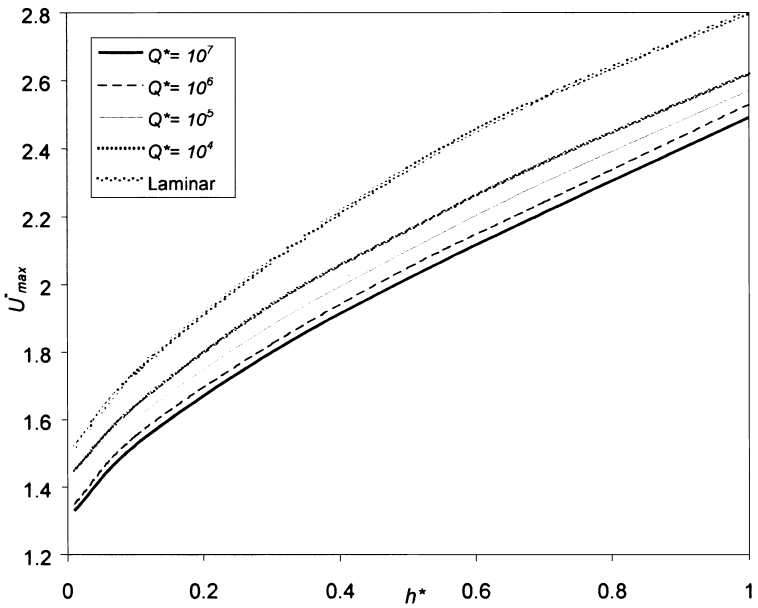

Fig. 6. Ratio between maximum velocity u_{max}, with debris and uniform velocity U_0 in case of no debris.

expression:

$$d^* = d^*(Q^*, h^*). \tag{35}$$

This means it is always possible to provide the proper values of d^*, once h^* and the discharge Q^* are known. Eq. (35), properly stated, needs to be solved by finding the dimensionless water depth d^*, with which the dimensionless discharge Q^* is conveyed under the external forcing h^*. This is achieved through numerical integration of Eq. (27) for increasing water depths, until the correct value for d^* is found. Although the procedure is numerical, its results are universal, i.e. they are valid for any case, once the relevant physical variables are properly transformed into non-dimensional ones. The results can be summarized in a chart where the correct d^* are plotted vs. h^*, having Q^* as parameter. The differences between water depth and bed shear for free surface and Couette (with floating debris) flows are calculated. Once d^* is known, T^* is easily found, by the first equality in Eq. (34), which still holds for turbulent motion. In Figs. 5a,b and 6 the resulting charts are shown. For the sake of clearness, only four different values of Q^* are shown, spanning over four orders of magnitude (i.e. from 10^4 to 10^7). Values within this range are well representative for the hydraulic conditions of a wide river having unit width discharges ranging from 10^{-2} to 10 $m^2\ s^{-1}$. Fig. 5a shows the correct values of d^*, for both turbulent and laminar flow (Eq. (33)). The laminar flow curve is indeed very similar to the turbulent ones. This confirms the expected trend, analytically derived for the laminar case. In fact, the chart clearly shows a decrease in water depth, due to the additional shear on the upper surface. The curves for turbulent flows are slightly different from each other, depending on the Q^* value. From a theoretical point of view, different curves should be adopted for different dimensionless discharges. The greater the latter, the smaller the decrease in the water depth, for the same dimensionless debris weight, h^*. From the application perspective, the results are almost equivalent and an average curve can be used.

Fig. 5b shows the correct values of T^*. Once again, the analytical results for laminar flow are qualitatively confirmed and the shear stress is larger, for a fixed discharge, with respect to the analogous free surface flow. It is evident that the different curves in Fig. 6 although different, are very close to each other. Also in this case an average fitting curve can be used. As stated before, the debris weight can be varied as well as its thickness. Assuming, as an example, a specific debris weight of 5 kN m^{-1}, some considerations can be done. The range of the h^* values in Fig. 5a and b is

0.01–1. This corresponds to a layer of debris ranging from approximately 0.5 to 200% of the free surface water depth h_0. Having $h_0 = 1$ m, the debris thickness ranges from 5 to 2 m. The most likely values for such thickness is of course expected to be somewhere in the middle of this range, which however looks as a reasonable one. Looking at Fig. 5a for a debris thickness of 0.4 m, which corresponds to $h^* = 0.2$, the water depth reduction is almost independent of the discharge Q^*, thus giving a ratio of about 93% with respect to the free surface value h_0. Conversely the bed shear results in about 110% of the corresponding free surface τ_0. For a debris thickness of 1 m ($h^* = 0.5$), the water depth and shear stress would reach 84 and 135%, respectively, of the corresponding values when no debris is present. To give an idea about the shape of the two curves, two equations are shown here, for d^* and T^* vs. h^*, in turbulent flows, obtained by fitting the average values of d^* for different Q^*. The dimensionless depth results given by

$$d^* = 1 - 0.29h^*, \tag{36}$$

yielding an explained variance, R^2, of 0.98. As expected, it tends to 1 for a zero debris weight. The expression for the dimensionless shear stress is given by

$$T^* = 1 + 0.71h^*, \tag{37}$$

with R^2 practically equal to one (0.998).

It is seen that a quite linear dependence exists between the increase in the debris weight and the corresponding changes in channel depth and bed shear. This result is particularly interesting especially when looking at bed sediment stability and transport!

As far as the maximum flow velocity or debris velocity is concerned, its increase is assessed after introducing

$$U^*_{\max} = \frac{u_{\max}}{U_0}, \tag{38}$$

which gives the ratio of maximum velocity to free surface velocity. Its trend is shown in Fig. 6.

As seen in Fig. 6 $U^*_{\max}$ is maximum for laminar flows, as expected, because of the high value of the velocity derivative in the field, not smoothed by turbulence. Referring to the former example, for h^* equal to 0.2 and 0.5, and $Q^* = 10^6$, the maximum velocity is $\sim$1.7 and $\sim$2 times the analogous free surface velocity, respectively. If the given discharge per width unit of 1 $m^2\,s^{-1}$ would be conveyed in a river with a slope of, say, 10^{-4}, U_0 would reach the value of about 1.1 $m\,s^{-1}$. The maximum related velocity under floating debris transport would raise to 1.85 and 2.2 $m\,s^{-1}$, respectively!

Generally speaking, the figures and trend enlightened with this approach would require some validation. Particularly, one is interested in understanding whether and, eventually under which conditions, the proposed approach is applicable to fairly describe the main flow features. This issue requires indeed some experimental testing in channels, before the results can be adopted. From a qualitative point of view, it is however shown that the floating debris is expected to someway alter the velocity distribution and the bed shear as well. Also, the debris is expected to move faster than the average current velocity, thus possessing a greater amount of momentum. Such findings should be taken into account in channels with heavy yields of debris, either when designing dams, bridges or decks or in controlling debris yield by trapping nets or rakes.

5. Conclusions

Flood flows in rivers are influenced by the action of floating bodies on the surface, exerting an additional force in the flow direction. This issue has been addressed here through a simplified approach for very wide channels covered by a homogeneous solid carpet of floating debris. Its effects have been investigated for both theoretical laminar regime, enlightening the main flow feature and the more likely turbulent regimes. A turbulence model has been described, which fits well the available experimental profiles. Adopting such model, curves are drawn, in the proper parameter space, assessing the dynamics of this kind of Couette like flows. The velocity profiles exhibit a non-negligible deviation from the free surface condition. This also implies that the fluid discharge increases, for a given water depth. Conversely, a fixed fluid discharge is conveyed with different water depths. Indeed, the more the debris weights, the shallower the flow. Furthermore, the related bed shear monotonically increases with the weight of debris. The results are of some interest, since they show, at

least from a qualitative point of view, the changes in the flow characteristics, when governed by an external forcing, i.e. the debris. This appears to be much more important when dealing with the morphodynamics of river channels under floating debris transport. In this respect it is clear that 1D or 2D shallow water approaches cannot give a reliable description of the shear stress patterns inside the fluid domain and ultimately a correct estimate of the sediment movement. The results of this research are therefore of utmost importance for a future deduction of more synthetic parameters for shallow water models and for movable bed models. As a drawback, the presented approach only deals with smooth surface, i.e. channels with very small roughness. In case some measurements were available for floating debris transport, for river channels and different roughness, the theory could be extended and tested for a broader range of cases and more comprehensive conclusions could be drawn. It is the opinion of the authors that the proposed method, although preliminary, yields some clues about the fundamental features of the investigated phenomenon and raises some interesting questions for the development of the related research.

Acknowledgements

The authors here acknowledge an anonymous reviewer, whose interesting suggestions and requests helped in giving the paper a more readable format and in pointing out the main features and possible applications of the approach here proposed in the field of numerical hydrology.

References

Abbe, T.B., Montgomery, D.R., 1996. Large woody debris jams, channel hydraulics and habitat formation in large rivers. Regul. Rivers: Res. Manage. 12, 201–221.

Alfonsi, G., Passoni, G., Pancaldo, L., Zampaglione, D., 1998. A spectral finite difference solution of the Navier Stokes equations in three dimensions. Int. J. Numer. Meth. Fluids 28, 129–142.

Andrus, C.W., Long, B.A., Froehlich, H.A., 1988. Woody debris and its contribution to pool formation in a costal stream 50 years after logging. Can. J. Fisheries Aquat. Manage. 45, 2080–2086.

Bilby, R.E., Ward, J.W., 1989. Changes in characteristics and function of woody debris with increasing size of streams in western Washington. Trans. Am. Fishery Soc. 118, 368–378.

Braudrick, C.A., Grant, G.E., 2000. When do logs move in rivers ? Water Resour. Res. 36 (2), 571–583.

Braudrick, C.A., Grant, G.E., Ishikawa, Y., Ikeda, H., 1997. Dynamics of wood transport in streams: a flume experiment. Earth Surf. Process. Landforms 22, 669–683.

Bryant, M.D., 1983. The role of management of woody debris in west coast salmonid nursery streams. North American Journal of Fisheries Management 3 (3), 322–330.

Chapman, D.R., Kuhn, G.D., 1986. The Limiting behavior of turbulence near a wall, J. of Fluid Mechanics 170, 265–292.

Diehl, T.H., (1997). Potential drift accumulation at bridges, U.S. Department of Transportation, Federal Highway transportation, FHWA-RD-97-028.

Egiazaroff, J.V., 1965. Calculation of nonuniform sediment concentrations. Proc. Am. Soc. Civil Engrs 91 (HY4).

El Telbany, M., Reynolds, A.J., 1980. Velocity distribution in plane turbulent channel flow. JFM 100, 1–29.

Ginanni, F., Becchi, I., Castelli,F., 2000. Cinematica dei detriti arborei nelle correnti a pelo libero (Cinematic of woody debris in free surface currents). IDRA 2000, XXVII Congress of Hydraulics and Hydraulic Constructions, Genova, 12–15 September, vol. 1, pp. 271–279, paper in Italian language.

Harmon, M.E., et al., 1986. Ecology of coarse woody debris in temperate ecosystems. In: MacFadyen, A., Ford, E.D., et al. (Eds.), Advance in Ecological Resources, vol. 15. Harcourt Brace Jovanovich, New York, pp. 133–302.

Keller, E.A., Swanson, F.J., 1979. Effects of large organic material on channel form and fluvial processes. Earth Surf. Process. Landforms 4, 361–380.

Knight, D.W., Patel, H.P., 1985. Boundary shear in smooth rectangular ducts. J. Hydraul. Engng 111 (1), 29–47.

Lienkaemper, G.W., Swanson, F., 1987. Dynamics of large woody debris in streams of in old growth Douglas-fir forests. Can. J. Forest Res. 17, 150–156.

Lundbladh, A., Johansson, A., 1991. Direct simulation of turbulent spots in plane copuette flows. J. Fluid Mech. 194, 15–44.

Manga, M., Kirchner, 2000. Stress partitioning in streams by large woody debris. Water Resour. Res. 36 (8), 2373–2379.

Murgatroyd, A.L., Ternan, J.L., 1983. The impact of afforestation on stream bank erosion and channel form. Earth Surf. Process. Landforms 8, 357–369.

Passoni, G., Alfonsi, G., Tula, G., Cardu, U., 1999. A wavenumber parallel computational code for the numerical integration of the Navier Stokes Equation. Parallel Comput. 25, 593–611.

Perham, R.E., 1987. Floating debris control: a literature review. US Army Cold Region Research and Engine Laboratory, Technical Report REMR-HY-2, p. 63 (available from the National Technical Information Service, Springfield, VA 22161).

Perham, R.E., 1988. Elements of floating debris control, systems, Washington DC. US Army Corp of Engineer, Technical Report REMR-HY-3, p. 69.

Prandtl, L., 1925. Bericht über Untersuchungen zur ausgebildeten Turbulenz. Z. Abgew. Math. Mech. (ZAMM) 5, 136–139.

Rhodes, D.G., Knight, D.W., 1994. Distribution of shear force on

boundary of smooth rectangular duct. J. Hydraul. Engng 120 (7), 787–807.

Schlichting, H., 1960. Boundary Layer Theory, McGraw Hill, New York.

Shermann, F., 1990. Viscous Flow, McGraw Hill, New York.

Shields, A., 1936. Anwendung der Ahnlichkeitsmechanik und turbulenzforschung auf die Geschiebebewegung. Mitteil. Preuss. Versuchsanst. Wasser, erd, Schiffsbau, Berlin, no. 26, Translation of W.P. Ott and J.C. Van Vehelen, US Department of Agriculture, SCS Coop lab., California Institute of Technology.

Shields, D.F., Gippel, C.J., 1995. Prediction of effects of woody debris removal on flow resistance. ASCE J. Hydraul. Engng 121 (4), 341–354.

Spalding, D.B., 1961. A single formula for the law of the wall. J. Appl. Mech. 28, 455–458.

Yalin, M.S., 1971. Theory of Hydraulic Models, Mac Millan, London.

Yalin, M.S., 1982. Mechanics of Sediment Transport, Pergamon Press, Oxford.

Young, W.J., 1991. Flume study of the hydraulic effects of large woody debris in lowland rivers. Regul. Rivers: Res. Manage. 6, 203–211.

Wilcox, D.C., 1993. Comparison of two-equation turbulence models for boundary layers with pressure gradient. AIAA J. 31, 1414–1421.

Van Driest, E.R., 1956. On turbulent flow near a wall. J. Aeronaut. Sci. V (23), 1007–1011.